Simulations of the scintillation-producing irregularities in high-latitude plasma patches

N. A. Gondarenko[1] and P. N. Guzdar[1]

Received 8 September 2006; revised 18 October 2006; accepted 24 October 2006; published 29 November 2006.

[1] The simulation study of mesoscale scintillation-producing irregularities obtained with the 3-D nonlinear model for the structuring by the gradient-drift instability (GDI) and the velocity-shear-driven instability in high-latitude plasma patches is presented. We have identified four groups of mesoscale structures based on the structuring mechanisms. The amplitudes of the scintillation-producing irregularities have been described with a normalized irregularity index which is proportional to the scintillation index S_4 and accounts for the greatest variability in ionospheric scintillation. We have demonstrated that the dominant mechanism which can lead to intense scintillation is related to the patch structuring by the primary GDI and high plasma density in a patch. In the velocity shear simulations, the values of the irregularity index are found to be weaker than those produced in the simulations with no shear. The relations between the magnitudes of the simulated electric field and density irregularities have been derived for each category. **Citation:** Gondarenko, N. A., and P. N. Guzdar (2006), Simulations of the scintillation-producing irregularities in high-latitude plasma patches, *Geophys. Res. Lett.*, *33*, L22107, doi:10.1029/2006GL028033.

1. Introduction

[2] The observations of the plasma structures at high latitudes associated with polar cap ionization patches have identified large-scale (hundreds of kilometers) enhanced plasma density regions referred to as patches and auroral blobs and small-scale/mesoscale irregularities (with scale sizes ranging from a few tens of kilometers to tens of meters) embedded in the large-scale structures [*Weber et al.*, 1984, 1986; *Basu et al.*, 1990; *Kivanç and Heelis*, 1997, 1998; *Coley and Heelis*, 1998]. These kilometer-scale irregularities produce scintillation phenomena in trans-ionospheric radio signals.

[3] The observations show that patches are associated with the scintillation caused by mesoscale structures [*Buchau et al.*, 1985, 1988]. The authors have investigated the ionospheric structures in polar cap and indicated that the patches are the dominant cause of scintillation events. From the observational studies, *Tsunoda* [1988] have concluded that high-latitude small-scale irregularities generated by the GDI are associated with macroscale plasma structures which determine the formation of mesoscale structures. Later, *Basu et al.* [1990] have established that mesoscale structures develop at the edges of macroscale structures (patches) through the gradient-drift instability process. The mesoscale irregularities have been also identified in the velocity shear regions associated with nightside auroral arcs [*Basu et al.*, 1988]. The study of the distribution and dynamics of mesoscale density irregularities in the dayside auroral region has been performed by measuring the effects of these irregularities on the amplitude scintillation [*Basu et al.*, 1998].

[4] The detailed observational studies of mesoscale structures have stimulated development of the numerical models. Recently, *Guzdar et al.* [1998], *Gondarenko and Guzdar* [1999, 2001, 2003, 2004a, 2004b], and *Gondarenko et al.* [2003] have convincingly demonstrated the nature of mesoscale structuring in high-latitude plasma patches by a combination of the primary GDI and secondary Kelvin-Helmholtz (KH) instability followed by the tertiary generation of shear flow within the patches. The magnitudes and spectral characteristics of the simulated density $\Delta N/N$ and electric field ΔE fluctuations have been studied by *Gondarenko and Guzdar* [2004a]. In the directions parallel and perpendicular to convection, the similarities in spectral slope distributions of both simulated [*Gondarenko and Guzdar*, 2004a] and observed [*Basu et al.*, 1990] $\Delta N/N$ and ΔE have been demonstrated. The amplitudes of the simulated density fluctuations and the relation between the magnitudes of ΔE and $\Delta N/N$ have been found to be in good agreement with the measured characteristics reported by *Basu et al.* [1990].

[5] To account for the large variability in the statistical and spectral characteristics of the satellite data by *Basu et al.* [1988, 1990], *Gondarenko and Guzdar* [2006] have combined two sources of the mesoscale structuring, namely the primary gradient drift instability and velocity-shear-driven instability (or Kelvin-Helmholtz instability), in their 3-D nonlinear model for the structuring in high-latitude patches. They have studied the interactions of the gradient-drift instability with the primary KH instability caused by the sheared flow perpendicular to the geomagnetic field and to the density gradient. The effects of these two dominant instabilities on mesoscale structuring at high latitudes have been investigated. It has been demonstrated that the strong anisotropy induced by the GDI in the density fluctuation spectra can be significantly reduced when the velocity-shear-driven instability is taken into account [*Gondarenko and Guzdar*, 2006]. This can result in production of small-scale turbulence and appears to be the dominant mechanism for isotropization of the density fluctuation spectra in the noon-midnight and dawn-dusk directions.

[6] In this paper, we present the simulations of mesoscale irregularities in high-latitude plasma patches obtained with the 3-D model for the nonlinear evolution of the primary GDI and velocity-shear-driven instabilities. The density

[1]Institute for Research in Electronics and Applied Physics, University of Maryland, College Park, Maryland, USA.

0094-8276/06/2006GL028033

Table 1. Simulations of High Latitude Plasma Patches

Patch Number	R	V, km/s	ν_{in}, s^{-1}	V_0	Patch/Grid Sizes in xy Plane, km
1	3	1	0.1	0	[200, 50]/[0.2, 0.1]
2	3	1	0.1	0	[400, 50]/[0.4, 0.1]
3	3	1	0.1	0	[400, 50]/[0.8, 0.1]
4	3	0.5	0.1	0	[400, 100]/[0.4, 0.1]
5	3	1	0.1	0	[400, 400]/[0.8, 0.8]
6	2	1	0.1	0	[200, 50]/[0.2, 0.1]
7	2	1	0.1	0	[400, 50]/[0.4, 0.1]
8	2	0.5	0.1	0	[400, 50]/[0.2, 0.1]
9	2	1	0.1	0	[400, 400]/[0.4, 0.4]
10	2	1	0.02	0	[400, 400]/[0.4, 0.4]
11	4	1	0.1	3	[400, 400]/[0.8, 0.8]
12	3	1	0.1	2	[400, 400]/[0.8, 0.8]
13	3	1	0.1	2.25	[400, 400]/[0.8, 0.8]
14	3	1	0.1	2.5	[400, 50]/[0.4, 0.1]
15	2	1	0.1	1.5	[400, 50]/[0.4, 0.1]
16	3	1	0.1	0.5	[400, 400]/[0.8, 0.8]
17	3	1	0.1	1	[400, 400]/[0.8, 0.8]
18	2	1	0.1	0.5	[400, 400]/[0.4, 0.4]
19	2	1	0.1	0.5	[400, 50]/[0.4, 0.1]

irregularity is the most important quantity which controls ionospheric scintillation. The amplitude of the scintillation-producing irregularities has been described using the irregularity indices I_4 derived from the density fluctuations of 19 patch simulations. We identify four groups of mesoscale structures based on the structure mechanisms and initial conditions. We show the average values of the irregularity index characterizing the mesoscale irregularities for each patch and the variation of the irregularity indices in the directions parallel and perpendicular to the direction of convection for the most representative patches from each group. The relationships between the magnitudes of ΔE and $\Delta N/N$ are derived for each category of mesoscale structures.

2. Simulation Results

[7] The scintillation method is used to study the ionosphere by measuring the fluctuations of radio signal traversed through an irregular medium. The key quantity, which contributes to the variability of ionospheric scintillation, is the density irregularity $\langle \Delta N^2 \rangle$. The scintillation index S_4 is proportional to the density fluctuations, $S_4^2 \sim \langle \Delta N^2 \rangle$ [*Rino*, 1979]. The intensity of amplitude scintillation is usually expressed by using indices written in terms of power S_4 or in terms of amplitude S_2 of radio waves [*Briggs and Parkin*, 1963], $S_4 = (\overline{p^2})^{1/2}/\bar{P}$, $S_2 = (\overline{a^2})^{1/2}/\bar{A}$, where $P = A^2$ is the power, $\bar{P}$ is the mean power, A is the amplitude, $\bar{A}$ is the mean amplitude, $a = A - \bar{A}$, and $p = P - \bar{P}$. Here S_2 is the root-mean-square deviation of the amplitude normalized by the mean amplitude and S_4 is the root-mean-square deviation of the power, similarly normalized. There is a linear dependence between index S_4 and S_2, $S_2 = 0.52 S_4$ [*Briggs and Parkin*, 1963]. In this study, we describe the amplitudes of the scintillation-producing irregularities with a normalized irregularity index I_4 estimated as $I_4 = (1/0.52)\sqrt{\overline{(\Delta N/N)^2}}$ or using the above expression for S_4 with $p = N^2 - \overline{N^2}$.

[8] The scintillation-producing irregularities have been categorized based on the structuring mechanisms. The first two groups are the mesoscale structures associated with the primary GDI and secondary KH instability and differ by the maximum plasma density in a patch. The second two groups are the simulations representing the strong/weak velocity shear category and associated with the primary GDI and velocity-shear-driven instability [*Gondarenko and Guzdar*, 2006]. The simulations in each category differ in space resolution, various values of the convection velocity **V** in the frame of the neutral wind velocity V_n and ion-neutral collisions ν_{in} as shown in Table 1. The values of ν_{in} are at the height of the density peak (near the F peak height z = 400 km) [*Gondarenko and Guzdar*, 2004b, Figure 1a].

[9] In Figures 1a and 1b, we show the values of I_4 for the four structure categories in the noon-midnight direction of convection (x) and dawn-dusk (y) direction perpendicular to convection, respectively. The corresponding values have been obtained for each patch near the density peak in the vertical z direction along the magnetic field. The first two categories are the simulations of the primary GDI with higher, R = 3 (filled circles) and lower R = 2 (filled boxes), plasma density. Here R is a ratio of the maximum density within the patch to the background density. The bars in Figure 1 indicate the standard deviation. The values of I_4 and amplitudes of the density and electric field fluctuations averaged over each patch in the x and y directions are shown in Figures 1c and 1d. One can see that the values of I_4 are greater for the simulations with the higher maximum density, R = 3. The mean irregularity index $\langle I_4 \rangle$ is 0.37 ± 0.03 and 0.26 ± 0.03 for the first and second groups, respectively. The normalized amplitudes of the density fluctuations $\Delta N/N$ are also greater for R = 3 (∼20%) than that for R = 2 (∼12%).

[10] In these two groups, the magnitudes of the electric field fluctuations ΔE_y in the direction perpendicular to convection are larger than the ΔE_x magnitudes in the direction of convection, as observed by *Basu et al.* [1990] and demonstrated in the simulations for the mesoscale structuring by the primary GDI by *Gondarenko and Guzdar* [2004a]. One interesting feature in both simulations with

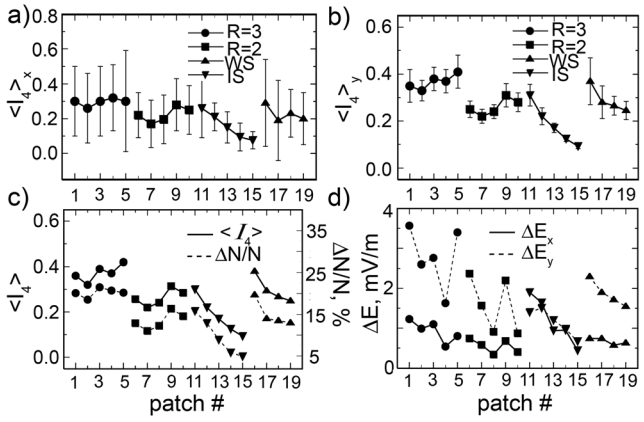

Figure 1. The values of I_4 for the simulations of the primary GDI with higher/lower plasma density, R = 3/2 (filled circles/boxes), and the simulations of the combined GDI and velocity-shear-driven instabilities with stronger/weaker shear (IS/WS-down/up triangles) in the directions (a) parallel and (b) perpendicular to the direction of convection. The averaged values of (c) I_4 and $\Delta N/N$ and (d) ΔE_y and ΔE_x.

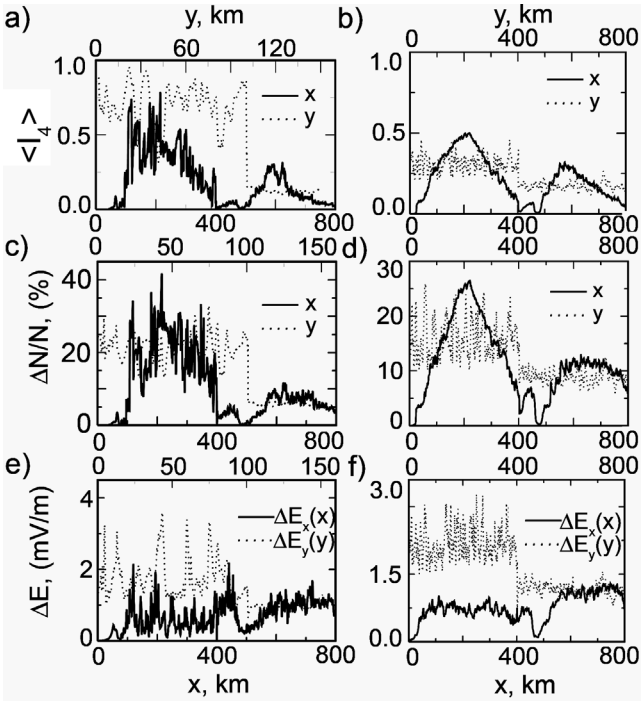

Figure 2. The variations of I_4, $\Delta N/N$, and ΔE for patches without/with shear (a, c, e) #4/#14 are shown with solid lines from 0/400 to 400/800 km in the x direction of convection and dotted lines from 0/100 to 100/160 km in the y direction perpendicular to convection and (b, d, f) for patches #9/#13 with solid and dotted lines from 0/400 to 400/800 km and in the x and y directions, respectively.

$R = 3$ and $R = 2$ is a decrease in the electric field fluctuation amplitudes for patches #4, #8, and #10. Note that first two simulations have been produced with the convection velocity of ~500 m/s which is two times smaller than that in the other simulations for these two categories and the third simulation is for the smaller value of ν_{in} at the density peak in z that can be associated with the event for the solar minimum.

[11] The next two groups are for the velocity shear simulations associated with the primary GDI and velocity-shear-driven instabilities [*Gondarenko and Guzdar*, 2006] with stronger/weaker shear (down/up triangles in Figure 1). In this model, the new equilibrium has two dominant drives, a sheared flow perpendicular to the geomagnetic field and density gradient across the shear. To derive the equilibrium velocity shear, we use the equilibrium condition which follows from vorticity equation [*Gondarenko and Guzdar*, 1999, 2006]. Thus for the KH instability within the equilibrium we have defined, the equilibrium potential is $\phi_0(x) = \int V_0/N_0(x)dx$, where V_0 is the parameter which controls the magnitude of the equilibrium velocity shear V_0/L, L is the velocity gradient scale length, and $N_0(x)$ is the equilibrium density. *Basu et al.* [1988] have observed the intense and moderate velocity shear regions with shear frequencies varying between 3 and 10 Hz and 0.1 and 1 Hz, respectively. In the third group simulations, the strongest velocity shear is about 0.1 s^{-1} (patch #11, $R = 4$) for the velocity gradient scale length of ~30 km, and the smallest shear frequency 0.022 s^{-1} is for the patch #15.

[12] The values of I_4 and the magnitudes of $\Delta N/N$ for patches #12–#14 ($R = 3$) decrease with an increase in the initial shear. It is interesting to note that in the directions parallel and perpendicular to convection, the ΔE magnitudes are similar. In these simulations, stronger shear results in production of small-scale turbulence that leads to an increase in dissipation at small scales, and reduces anisotropy in the density fluctuation spectra in the noon-midnight and dawn-dusk directions [*Gondarenko and Guzdar*, 2006]. In the velocity shear regions, scintillations are expected to be weaker than those associated with GDI and high plasma density [*Basu et al.*, 1998]. In the velocity shear simulations with two combined primary instabilities, when the KH instability dominates the GDI, the irregularity indices are less than those for the first two categories, and this can lead to a weaker scintillation. The structures in the last group have been produced in the weak shear simulations with shear frequencies 0.02–0.01 s^{-1}. In these simulations, the GDI dominates the KH instability, and the values of I_4 and the corresponding values of the density and electric field fluctuations exhibit behavior similar to those obtained in the simulations with no shear.

[13] To demonstrate the variations of I_4, $\Delta N/N$, and ΔE within a patch in the directions parallel (x) and perpendicular (y) to convection, we show simulations without/with shear in Figures 2a, 2c, and 2e for patches #4/#14 with solid lines from 0/400 to 400/800 km in the direction of convection and dotted lines from 0/100 to 100/160 km in the direction perpendicular to convection. In Figures 2b, 2d, and 2f, we show simulations without/with shear for patches #9/#13 with solid and dotted lines from 0/400 to 400/800 km in the x and y directions, respectively. In both directions x and y, the values of I_4 in the simulations with no shear are greater than those in the simulation with stronger shear, with a ratio of almost two between the irregularity indices. One can see that within a patch, the amplitude of the irregularities increases ($I_4 > 0.5$) due to the irregularities produced by the dominant GDI, and that can lead to intense scintillation.

[14] In Figures 3a, 3b, and 3c we show the relationship between the $\Delta N/N$ and ΔE fluctuations obtained in the simulations of the GDI (the first two categories with $R = 3$ and $R = 2$) and with the KH instability with stronger shear (the third category) and weak shear (the fourth category), respectively. In these Figures, a straight-line provides the relationship between $\Delta N/N$ and ΔE_y (solid line) and ΔE_x (dashed line). For the simulations with the primary GDI, the relation between the magnitudes of ΔE_y and $\Delta N/N$ confirms the relation obtained by *Basu et al.* [1990] from the observations. Also, the observations show that the ΔE magnitudes in the dawn-dusk direction are greater than ΔE in the noon-midnight direction. However, in our strong shear simulations, the ΔE magnitude is only a few millivolts per meter, though observations [*Basu et al.*, 1988] show a significant increase in the electric field fluctuations associated with velocity shear in the auroral oval. Thus one can assume that some other mechanism has to be invoked to explain the dramatic increase in the electric field fluctuations in the velocity shear regions associated with nightside auroral arcs.

[15] In conclusion, we have presented the simulation study of mesoscale irregularities in high-latitude plasma patches obtained with the 3-D model for the nonlinear

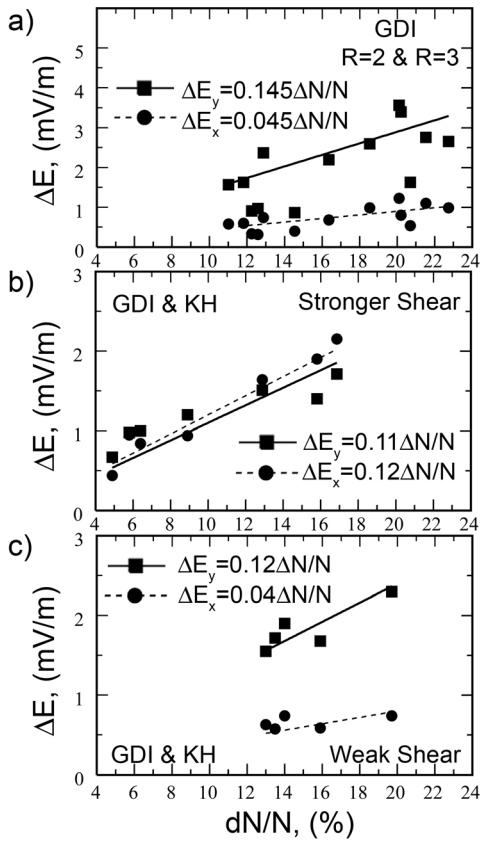

Figure 3. The relationship between the $\Delta N/N$ and ΔE fluctuations obtained in the simulations of (a) the GDI (with $R = 3$ and $R = 2$) and with the KH instability (b) with stronger shear and (c) weak shear.

evolution of the primary GDI and velocity-shear-driven instabilities. We have identified four groups of mesoscale structures based on the structuring mechanisms. Using the irregularity indices derived from the density fluctuations of 19 patch simulations, we have described the amplitude of the scintillation-producing irregularities. We have demonstrated that the dominant mechanism which can lead to intense scintillation is related to the patch structuring by the primary GDI and high plasma density in a patch. It has been found that values of the irregularity index I_4 are proportional to the maximum plasma density in a patch for the simulations with the primary GDI. In the simulations with stronger shear, the values of the irregularity index are found to be weaker than those produced in the simulations with no shear. The relations between the magnitudes of ΔE and $\Delta N/N$ have been derived for each category of mesoscale structures and compared to the observations by *Basu et al.* [1990].

[16] **Acknowledgments.** This research was supported by the NSF under grant ATM-0437174 and in part by the NSF cooperative agreement ACI-9619020 through computing resources provided by the NPACI San Diego Supercomputer Center and Pittsburgh Supercomputer Center.

References

Basu, S., E. MacKenzie, P. F. Fougere, W. R. Coley, N C. Maynard, J. D. Winningham, M. Sugiura, W. B. Hanson, and W. R. Hoegy (1988), Simultaneous density and electric field fluctuation spectra associated with velocity shears in the auroral oval, *J. Geophys. Res.*, *93*, 115.

Basu, S., E. MacKenzie, W. R. Coley, J. R. Sharber, and W. R. Hoegy (1990), Plasma structuring by the gradient drift instability at high latitudes and comparison with velocity shear driven processes, *J. Geophys. Res.*, *95*, 7799.

Basu, S., E. J. Weber, T. W. Bullett, M. J. Keskinen, E. MacKenzie, P. Doherty, R. Sheehan, H. Kuenzler, P. Ning, and J. Bongiolatti (1998), Characteristics of plasma structuring in the cusp/cleft region at Svalbard, *Radio Sci.*, *33*, 1885.

Briggs, B. H., and J. A. Parkin (1963), On the variation of radio star and satellite scintillation with zenith angle, *J. Atmos. Terr. Phys.*, *25*, 339.

Buchau, J., E. J. Weber, D. N. Anderson, H. C. Carlson, J. G. Moore, B. W. Reinisch, and R. C. Livingston (1985), Ionospheric structures in the polar cap: Their origin and relation to 250 MHz scintillation, *Radio Sci.*, *20*, 325.

Buchau, J., W. Reinisch, D. N. Anderson, E. J. Weber, and C. Dozois (1988), Polar cap plasma convection measurements and their relevance to the modeling of the high-latitude ionosphere, *Radio Sci.*, *23*, 521.

Coley, W. R., and R. A. Heelis (1998), Structure and occurrence of polar ionization patches, *J. Geophys. Res.*, *103*, 2201.

Gondarenko, N. A., and P. N. Guzdar (1999), Gradient drift instability in high latitude plasma patches: Ion inertial effects, *Geophys. Res. Lett.*, *36*, 3345.

Gondarenko, N. A., and P. N. Guzdar (2001), Three-dimensional structuring characteristics of high-latitude plasma patches, *J. Geophys. Res.*, *106*, 24,611.

Gondarenko, N. A., and P. N. Guzdar (2003), Structure of turbulent irregularities in high-latitude plasma patches—3D nonlinear simulations, in *Disturbances in Geospace: The Storm-Substorm Relationship*, *Geophys. Monogr. Ser.*, vol. 142, pp. 205–215, AGU, Washington, D. C.

Gondarenko, N. A., and P. N. Guzdar (2004a), Density and electric field fluctuations associated with the gradient drift instability in the high-latitude ionosphere, *Geophys. Res. Lett.*, *31*, L11802, doi:10.1029/2004GL019703.

Gondarenko, N. A., and P. N. Guzdar (2004b), Plasma patch structuring by the nonlinear evolution of the gradient drift instability in the high-latitude ionosphere, *J. Geophys. Res.*, *109*, A09301, doi:10.1029/2004JA010504.

Gondarenko, N. A., and P. N. Guzdar (2006), Nonlinear three-dimensional simulations of mesoscale structuring by multiple drives in high-latitude plasma patches, *J. Geophys. Res.*, *111*, A08302, doi:10.1029/2006JA011701.

Gondarenko, N. A., P. N. Guzdar, J. J. Sojka, and M. David (2003), Structuring of high latitude plasma patches with variable drive, *Geophys. Res. Lett.*, *30*(4), 1165, doi:10.1029/2002GL016437.

Guzdar, P. N., N. A. Gondarenko, P. K. Chaturvedi, and S. Basu (1998), Three-dimensional nonlinear simulations of the gradient drift instability in the high latitude ionosphere, *Radio Sci.*, *33*, 1901.

Kivanç, Ö., and R. A. Heelis (1997), Structures in ionospheric number density and velocity associated with polar cap ionization patches, *J. Geophys. Res.*, *102*, 307.

Kivanç, Ö., and R. A. Heelis (1998), Spatial distribution of ionospheric plasma and field structures in the high-latitude *F* region, *J. Geophys. Res.*, *103*, 6955.

Rino, C. L. (1979), Power law model for ionospheric scintillation: 1. Weak scatter, *Radio Sci.*, *14*, 1135.

Tsunoda, R. T. (1988), High-latitude F region irregularities: A review and synthesis, *Rev. Geophys.*, *26*, 719.

Weber, E. J., J. Buchau, J. G. Moore, J. R. Sharber, R. C. Livingston, J. D. Winningham, and B. W. Reinisch (1984), F layer ionization patches in the polar cap, *J. Geophys. Res.*, *89*, 1683.

Weber, E. J., J. A. Klobuchar, J. Buchau, H. C. Carlson Jr., R. C. Livingston, O. de la Beaujardiere, M. McCready, J. G. Moore, and G. J. Bishop (1986), Polar cap F patches: Structure and dynamics, *J. Geophys. Res.*, *91*, 12,121.

N. A. Gondarenko, and P. N. Guzdar, Institute for Research in Electronics and Applied Physics, University of Maryland, College Park, MD 20742, USA. (ngondare@umd.edu; guzdar@glue.umd.edu)